Wideband E-shaped Patch Antennas for Advanced Wireless Terminals

Yahya Rahmat-Samii[1] and Joshua M. Kovitz[1,2]
[1]Electrical and Computer Engineering Department, University of California Los Angeles, Los Angeles, CA, USA
[2]Advanced Concepts Laboratory, Georgia Tech Research Institute, Atlanta, GA, USA
Corresponding author: Yahya Rahmat-Samii (e-mail: rahmat@@ee.ucla.edu)

ABSTRACT Low-profile patch antennas have become ubiquitous in wireless terminals, especially as devices have become smaller and demand more functionality out of their RF subsystems. While their shape and size is attactive for many applications, their narrow bandwidth hinders their usage in many systems. With the rise of computer-aided design, many patch antenna design concepts have been presented with enhanced bandwidth capabilities. The E-shaped patch antenna, whose original shape presented in the early 2000's resembles the letter E, offers compelling performance with reasonable manufacturing complexity. In it most basic form, this antenna was linearly polarized and either wideband or dual-band. Over the last two decades, many variations of the E-shaped patch have been presented in literature: circularly polarized, miniaturized, frequency reconfigurable, or even polarization reconfigurable. This paper summarizes these efforts in realizing novel functionalities with a relatively simple design geometry.

INDEX TERMS antenna, circular polarization, dual-band, E-shaped, linear polarization, low-profile, miniaturization, patch antenna, reconfigurable, wideband.

I. INTRODUCTION

POSSIBLY one of the most prolific and widespread antenna design is the patch antenna. They are easy to implement and amenable to inexpensive mass fabrication using planar PCB fabrication processes. Not only this, their low profile allows them to be versatile for use in a wide range of applications where volume—especially in the vertical direction—is a major constraint. Their design also fits into a planar microstrip topology, which makes it straightforward to integrate into a microstrip circuit. In the array context, simple feeding structures can be easily created using microstrip lines to feed each array element. Patch antennas have been the go-to design for mobile handsets, base stations, laptops, GPS receivers, conformal antennas, and high gain antenna arrays.

The disadvantages of patch antennas have been recognized by the antenna community after their inception. The most prevalent issue designers face is a narrow bandwidth. Some designs also suffer from high cross polarization, low efficiency, and surface waves, but bandwidth remains as one of the most important issues for wireless applications. The narrow bandwidth arises from its operation that is similar to an electromagnetic cavity, which has many modes that resonate at discrete frequencies. Especially when electrically thin substrates are used, the resonances exhibit a high quality factor (Q), implying a narrow impedance matching bandwidth. In response to this issue, engineers investigated many different paths to overcome the bandwidth limitations.

This paper focuses on a particular design that has led to the development of a whole class of patch antennas which far surpass the bandwidths seen in canonical patch antennas (e.g. rectangular or circular patches). In general, one can extend the bandwidth of a single resonator by adding more resonators, leading to two (or more) resonant frequencies. There are many ways to accomplish this task. Multilayer stacked patches, parasitic resonators, clever patch shapes, and complex probes are among the most popular techniques. While each of these options have their advantages, great attention has been placed on techniques that maintain a single (PCB) layer, single-feed patch antenna structure, leading to reduced fabrication costs. Interestingly, an E-shaped patch has been found to provide exceptional performance in both radiation and impedance matching bandwidth [1]. An added bonus is that the E-shaped patch antenna operation has a nice explanation. Furthermore, the E-shaped patch antenna uses a single-layer and single-input.

The article is split into sections devoted to distinct evolutions of the E-shaped patch and all the capabilities made possible through the E-shape. After a brief description of the original E-shaped patch, as depicted in the center of Fig. 1, the latest developments to achieve many novel designs are discussed. The original E-shaped patch antenna is linearly polarized, wideband (or even dual-band), and symmetric about the horizontal axis. Recently, it has been shown that several modifications to the original E-shaped patch shape can lead to features such as circular polarization (CP), miniaturization, reconfigurability, and some combinations of each feature. In Fig. 1, the title of each design is shown in bold, and the design features are given below each title.

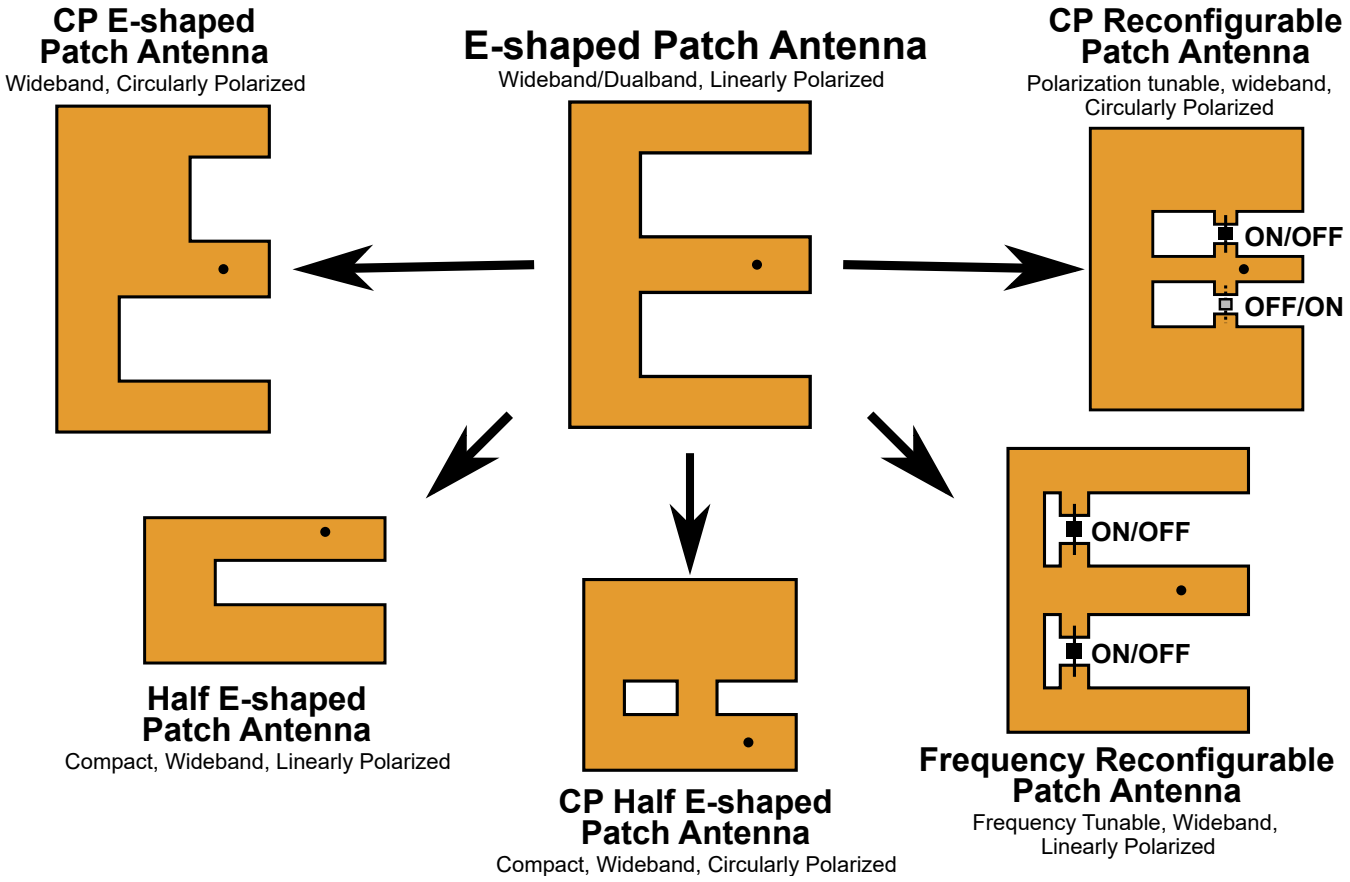

FIGURE 1. This paper focuses on the E-shaped patch antenna, which can be modified to achieve a wide variety of functionalities. This includes circular polarization, miniaturization, and reconfiguration.

II. E-SHAPED PATCH ANTENNA OPERATION

A. FUNDAMENTALS OF PATCH ANTENNAS

To better understand the operation of the E-shaped patch antenna, it is useful to revisit the operation of typical rectangular patch antennas. Starting with rectangular patch antennas allows us to reflect on the performance gains from the E-shaped patch, and it also provides a little background for those that might not be as familiar with patch antenna operation.

Since the 1980's, a significant effort was devoted to understand patch antennas and their operation. A rectangular patch antenna—as shown in Fig. 2—was among the first shapes that was investigated theoretically, and it remains one of the popular shapes used in industry. Using the cavity model, it has been shown that the impedance of this rectangular patch antenna can be approximately modeled as a parallel RLC circuit for thin substrates [2]. The parallel RLC circuit can be visualized in Fig. 2b, where the inductance $L_p = 0$. This model also assumes that we placed the probe along the y axis, where only y directed surface currents $\mathbf{J} = J_y\hat{y}$ are excited on the patch surface. The input resistance R_{in} and reactance X_{in} when $X_p = 0$ are plotted in Fig. 3a. Note that this particular patch is probe-fed with a coaxial cable; other feeding techniques will result in slightly different operation.

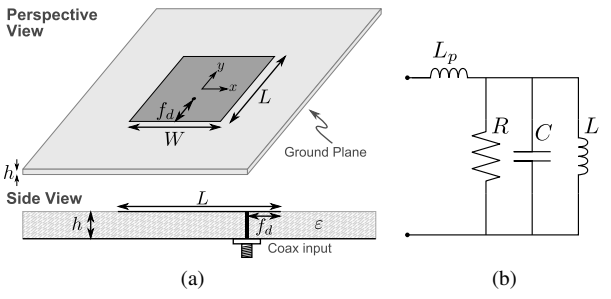

FIGURE 2. (a) Geometry of a simple single-layer, single-feed, probe-fed rectangular patch. (b) Circuit model (which can be generalized to most single-feed, single layer, probe-fed patch antennas).

As the substrate thickness increases, the probe inductance becomes a major factor in the patch operation. When including both the probe reactance and the parallel RLC circuit, the input impedance becomes [2]

$$Z_{in} = jX_p + \frac{R}{1 + j2Q(f_r - 1)} \tag{1}$$

where $X_p = \omega L_p$ represents the inductive probe reactance and the second term represents the RLC circuit impedance,

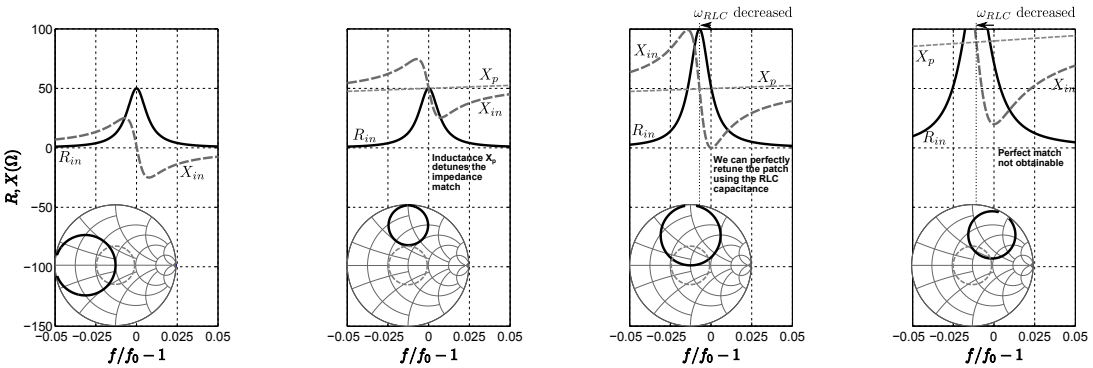

FIGURE 3. Impedance trends of the rectangular patch antenna. (a) Extremely thin substrates ($L_p \approx 0$). (b) Substrate height increases, and the designer has not reoptimized feed location and resonant frequency. (c) Using capacitive reactance of the RLC circuit to compensate for probe reactance. (d) Probe reactance too great to completely compensate with RLC capacitance.

which has both resistive and reactive components. Note also that we write this equation as a function of the frequency ratio $f_r = f/f_{RLC}$, where $\omega_{RLC} = 2\pi f_{RLC}$ is the resonant frequency of the RLC circuit. From a design perspective, engineers are most concerned with the design frequency f_0, and thus we plot the impedance curves in Fig. 3 relative to the design frequency f_0, rather than f_{RLC}. In this equation, Q is the quality factor of the RLC circuit alone. For a first-order approximation and for visualization purposes, the probe reactance can be nicely calculated using

$$X_p = \frac{\eta_0}{2\pi} k_0 h \left[\ln\left(\frac{2}{\sqrt{\varepsilon_r} k_0 a} \right) - \gamma \right] \tag{2}$$

where η_0 is the free-space impedance, h is the substrate thickness, a is the probe radius, k_0 is the free-space wavenumber, ε_r is the relative permittivity of the substrate, and γ is Euler's constant where $\gamma = 0.5772$. This is derived by calculating a probe reactance between two infinitely-sized parallel plates [2]. Note also that this equation assumes non-magnetic substrates having $\mu_r = 1$. Traditionally, the RLC circuit will resonate with a peak resistance and zero reactance at $\omega_{RLC} = 1/\sqrt{LC}$, as visualized in Fig. 3b. This probe inductance, however, changes the whole concept of resonance for this antenna. First, this inductance shifts the input reactance X_{in} curve upwards such that zero reactance is achieved at some frequency above $\omega_{RLC} = 1/\sqrt{LC}$ or potentially removes the zero-reactance frequency altogether. This can be visualized in Fig. 3b, where the probe reactance X_p shifts the input reactance curve X_{in} upwards so that $X_{in} = 0$ is not achieved. In this case, good impedance matching $S_{11} \leq -10$ dB is not achieved.

Engineers can retune the impedance matching by using the capacitance from the RLC circuit to cancel the probe reactance. This action is done by decreasing ω_{RLC} and decreasing f_d, which increases the radiation resistance[1] R. Despite rather large probe reactances on the order of 50Ω or greater, a zero-reactance point can still be achieved by using the capacitance embedded in the RLC circuit impedance to cancel the probe reactance. This can be visualized in Fig. 3c, where ω_{RLC} has been decreased and R has been increased to 100Ω. Unfortunately, there is a limit to the level of cancellation that can be achieved to cancel the probe reactance.

This limitation ultimately governs the bandwidth limitation of linearly polarized, rectangular patch antennas. For the given rectangular patch, the impedance bandwidth can be related to Q by [3]

$$BW_{LP} = \frac{\text{VSWR}_{\max} - 1}{\sqrt{\text{VSWR}_{\max}} Q} = \frac{0.707}{Q} \tag{3}$$

where $\text{VSWR}_{\max}$ is the maximum allowable VSWR, which is usually set to VSWR=2. Increasing the substrate thickness allows engineers to lower the RLC circuit's Q, providing for wider bandwidths (which is our desire). As the substrate thickness increases beyond a certain threshold, we can no longer cancel out the inductive probe reactance to provide $S_{11} \leq -10$ dB. In this situation, the impedances often appear as those seen in Fig. 3d, where the reactance minimum does not quite reach the $X_{in} = 0$ line. In this case, the feed point is at the edge of the patch, and there is nothing else that the designer can do to increase the radiation resistance, i.e. the reactance cannot be decreased any further. Eventually, the probe inductance becomes so dramatic that $S_{11} \leq -10$ dB can no longer be achieved for any frequency. This implies that the bandwidth of the rectangular patch (and many other canonical shapes) is ultimately limited by this maximum substrate thickness, where the Q can no longer be decreased. Above this thickness, the antenna can no longer be tuned appropriately, and designers must turn to other shapes for larger bandwidth capabilities. This is where the story gets exciting: the E-shaped patch can contribute a reactance that

[1] It should also be pointed out that the radiation resistance R can be tuned by changing the patch width W also, but the changes are somewhat limited because other undesirable features can arise. Engineers like to keep the width in the range of $0.4\lambda_g < W < 0.7\lambda_g$ for reasonable radiation efficiency and cross-polarization performance.

better compensates for this probe inductance and achieve even wider bandwidths.

B. USING AN E-SHAPE FOR WIDEBAND OR DUAL BAND PERFORMANCE

There are several techniques to avoid or further compensate for the probe inductance. A stacked patch antenna configuration [4], avoids this by using a driven patch and a coupled patch, thereby using a shorter probe feed. By shortening the probe feed, a smaller inductance is seen at the input port. The upper patch couples to the driven patch in an effort to provide another resonant frequency, which can extend the bandwidth. While this design avoids the probe inductance by using another layer, a multilayered antenna can have its own challenges in manufacturing and alignment.

Another technique to overcome the probe inductance is through the use of an L-shaped probe [5]. The L-shaped probe-fed antenna antenna utilizes an L-shaped probe that is capacitively coupled to the patch and overcomes the probe inductance by introducing some series capacitance seen at the input port. This design is able to get roughly 27% to 35% bandwidth with fairly high gain, which is comparable to other antennas in its class. However, this patch antenna can be tricky to fabricate and requires either a three dimensional manufacturing approach or a multilayered approach in order to construct it. This increases the cost and complexity for manufacturing, making it a less attractive candidate.

The addition of slots in the patch antenna also offers the possibility to obtain wide bandwidth. The basic idea is to take a typical single-layer, single-feed patch antenna (such as a rectangle) and cut out parts of the metal to generate interesting operational features. By cutting slots, new modes are excited which can either benefit or degrade the original patch performance. The important question is the choice of slot geometry that benefits our goals of wideband performance. Back in the early 2000's, our findings revealed that an E-shaped patch antenna [1], formed by cutting two rectangular slots to make an "E-shape" as seen in Fig. 4a, would allow us to signifcantly increase typical bandwidths seen in patch antennas. The advantage in this approach is that fabrication only entails a single round of metal layer processing on the top layer. The ground plane remains intact, with the only remaining task of inserting a coaxial probe to excite the antenna. The single feed input also simplifies the feeding process, where a simple coaxial cable can be connected to feed the antenna. Other similar types of slotted patch antennas include the U-slot antenna [6], [7] and a detailed comparison was presented in [8].

Our first observations found that the E-shaped patch geometry provided wide bandwidth in two manifestations: enabling thick substrates and adding an additional impedance matching resonance ($S_{11} = 0$). In the first full investigation [1] on the E-shaped patch, the findings revealed that there were two distinct modes of operation for the patch antenna. The two modes have different electric current distributions, as shown in Figs. 4b-4c. Like we mentioned previously, rectangular patch antennas—when probe-fed along the center of the patch width (y-axis)—will excite a current distribution with primarily y-directed currents. The additional slots do not signficantly disturb this mode and its resonant frequency. In other words, the resonant frequency for the typical rectangular "patch mode" is still dominantly controlled by the patch length L. This patch mode is illustrated in Fig. 4c. The insertion of the slots, however, allows the excitation of a new mode, where the currents meander around the slot. This slot mode is illustrated in Fig. 4b.

This additional slot mode is the most interesting feature of the E-shaped patch antenna. With this mode present, the patch antenna can operate with thick substrates (resulting in a lower quality factor Q), and the slot mode's impedance can be tuned to provide interesting operating characteristics such as dual-band or wideband operation. Recently, there have been interesting theoretical studies taken to understand this mode and how it contributes to the operation of the E-shaped patch antenna [10]. Using a transmission line model, researchers were able to demonstrate an equivalent circuit model for the E-shaped patch antenna. The fundamental operation is shown in the circuit of Fig. 5, where the familiar probe reactance ωL_p and patch mode impedance Z_r can be seen. For typical E-shaped patch antenna geometries, the new slot mode manifests as a reactive, parallel LC tank circuit whose impedance is Z_s. This slot mode impedance is primarily reactive, enabling a dynamic tuning capability that was not readily found in previous patch antenna designs.

Fig. 5b highlights the typical features of the impedances in a wideband E-shaped patch antenna design, where X_p, X_s, X_r, and R_r represent the probe reactance, slot mode reactance, patch mode reactance, and patch mode resistance, respectively. Like we have seen in the previous results, thick substrates can lead to very large probe reactances, e.g. 90Ω, which significantly impacts the operation of the patch antenna. This is clear in Fig. 5b, where the probe reactance X_p is large and linearly increases with frequency. The patch mode reactance and resistance exhibit the typical features seen in parallel RLC tank circuits, and the resonance of the patch mode impedance Z_r occurs at f_0. As for the slot mode impedance, Z_s, the resonance of this tank circuit often occurs lower than the resonant frequency of the patch mode. In other words, this tank circuit exhibits a capacitive reactance at f_0, which ultimately can be used to counteract the inductive probe reactance.

The E-shaped patch takes advantage of the probe reactance and slot mode reactances. Fig. 5c shows the total input impedance of the E-shaped patch $Z_{in} = Z_r + j\,(X_s + X_p)$. The total reactance from the probe, slot mode, and patch mode $X_p + X_s + X_r$ cancel at three frequencies. Comparing Figs. 5b-5c, this happens because the reactance from the probe and slot mode can actually reduce the reactance from the patch mode X_r. These three frequencies can also be visualized by the inset Smith chart in Fig. 5c, where the impedance intersects the horizontal axis. The dashed line on the Smith chart depicts the VSWR = 2 impedance contour,

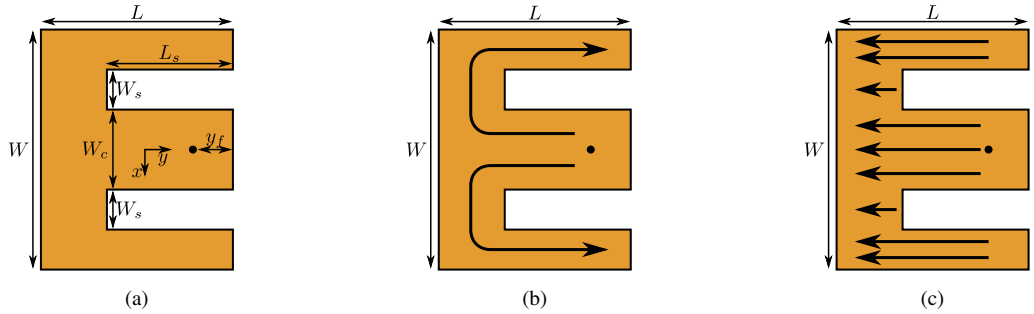

FIGURE 4. (a) E-shaped patch geometry. (b) Illustration of the slot mode electric current distribution. (c) Illustration of the radiating patch mode electric current distribution. Adapted from [9].

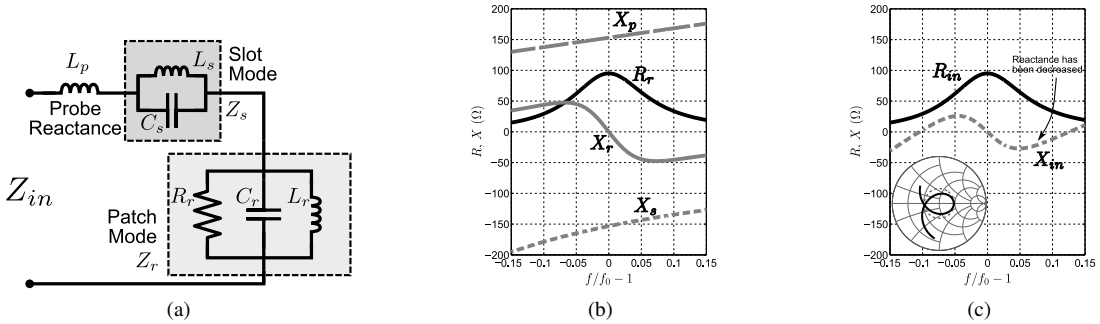

FIGURE 5. (a) A simplified circuit model for the E-shaped patch based on [10]. (b) Impedance and reactance contributions from each component in the circuit. (c) The input impedance (along with the Smith chart) of all components together, making a wideband patch antenna.

where good impedance matching is obtained for points inside the circle. As discussed in detail in [10], a wideband design would tune the geometry to achieve a VSWR=2.0 at f_0. Since the reactance is zero at f_0, the resistance R_r should be near 100Ω.

The probe and slot mode reactances also must be tuned with two objectives: $X_s = -X_p$ at f_0 and counteracting the patch mode reactance X_r for off-resonant frequencies. The probe reactance is controlled by changing the height, probe diameter, and probe location. In the case that the substrate height is fixed, this probe reactance is limited to a small range of values. The most intuitive approach in tuning the probe reactance is through adjusting the diameter of the probe feed. The location of the probe feed can also change the probe reactance [2] slightly, but this is difficult to quantify and is not intuitive. The slot mode, on the other hand, can be more readily tuned to compensate for the reactances. The slot width W_s, center bar width W_c, slot length L_s, and feed position y_f control this reactance.

If dual-band operation is desired, then the resonant frequencies (excluding f_0) become the focus for the designer. Since we can control R_r by the placement of the feed, we have the capability to shift the R_{in} curve in Fig. 5c up or down. We also can control the frequencies f_1 and f_2 by controlling the probe and slot mode reactances along with the Q of the patch mode.

TABLE 1. Design parameters for a wideband and dual-band E-shaped patch design (units in mm) [13]

	L	W	L_s	W_s	W_c	y_f
Wideband	52.0	82.0	48.0	20.0	4.0	13.0
Dual-band	54.0	46.0	47.0	20.0	4.0	13.0

Tuning the antenna is now evident for the E-shaped patch antenna and has been explained. As an example, we show two designs of the E-shaped patch antenna. The first is a wideband design, and the second is a dual-band design. To achieve the optimal performance, we employed a nature-inspired optimization technique, Particle Swarm Optimization (PSO) [11], [12], to explore the optimal design of this patch antenna concept for a given substrate thickness of $t = 15$mm. For the wideband design, PSO optimized the S_{11} performance throughout the band 1.8–2.4 GHz. In the dual-band design, on the other hand, the E-shaped patch was optimized to provide superior performance in the individual frequencies 1.8 and 2.4 GHz.

We highlight the final design parameters in Table 1. Typically, the optimal lengths for the E-shape are roughly $0.4\lambda_0$, while the E-shaped patch width W can vary significantly depending on the operation of the patch antenna. It has been our experience that the wideband designs often require

$W > \lambda_0/2$, while the dual-band designs can vary between $0.35\lambda_0 < W < 0.5\lambda$ (depending on the frequency separation). The extra width limits the usage of the E-shaped patch in array applications, which has been a subject of recent interest. In a following section, we discuss the possibility to miniaturize the E-shaped patch for a more suitable design in such cases.

Very good performance can be achieved with the E-shaped patch antenna. The measured impedance matching performance for the wideband and dual-band designs can be observed in Fig. 6a. The wideband design was able to achieve a measured $S_{11} \leq -10$dB bandwidth of 1.79–2.43 GHz (30.5%). This is much wider than typical bandwidths observed for single-layer, single-feed patch antennas. The dual-band design also exhibited desirable performance at the optimized frequencies of 1.8 and 2.4 GHz, with an $S_{11} \leq -18$dB for both frequencies.

The radiation patterns also exhibited good performance. For brevity, we only show the patterns for the wideband performance design in Fig. 7. In this figure, we show the patterns for the two principle planes (E-plane and H-plane) for two frequencies. The lower frequency (1.85 GHz) exhibits typical features for a rectangular patch, where typical beamwidths and cross-polarization levels are observed. The upper frequency (2.2 GHz) also has similar features. It should be noted that cross-polarization is often fairly noticeable when using thick substrates. The radiation from the probe (monopole-like radiation) accounts for these increases and is invariant of the patch shape. The insertion of slots to make the E-shape is also responsible for the increase in cross-polarization. Between the upper and lower frequencies of the patterns in Fig. 7, one notable difference is the increase in cross-polarization towards the horizon for the H-plane (Fig. 7d). Since the wideband design had a larger width, it is possible that a higher order mode resonates along the patch width W, radiating a difference pattern for the cross-polarization as observed.

III. OBTAINING CIRCULAR POLARIZATION

The original E-shaped patch discussed in the previous section demonstrated either a wideband or dual-band performance, but the antenna was linearly-polarized (LP) [1], [13]–[15]. The E-shaped patch design can be modified to create a wideband circularly polarized patch antenna which has many applications. Recently, researchers demonstrated that introducing an asymmetry in the slot configuration as seen in Fig. 8a, where one slot is shortened in length. By using asymmetric slots, the CP E-shaped patch design can excite an orthogonal polarization with quadrature phase, assuming that the proper geometry is used [16]. A follow-up research also demonstrated that it was equivalent to use a shorting bar to create circular polarization [12]. The "shorting bar" version is shown in Fig. 8b. For the cases studied, no major differences between the two geometries has been observed, although the "shorting bar" design is better suited to develop an RHCP/LHCP reconfigurable patch antenna, as discussed in a later section. For the rest of this section, we use the "shorting bar" version to demonstrate and explain the CP features within the design as an arbitrary choice.

TABLE 2. Design parameters for a CP E-shaped patch design (units in mm) [12]

L	W	L_s	W_s	W_c	y_f	W_b	$L_{s,2}$
39.2	94.8	30.2	14.5	9.3	14.6	5.0	3.9

To demonstrate the CP patch operation, we can investigate the electric surface currents $\mathbf{J}_s$ on the patch, plotting them against time. An example of these plots is shown for a representative CP E-shaped patch geometry in Fig. 9. Fig. 9a shows the electric surface currents at time $\omega t = \Omega_0$, where Ω_0 was chosen arbitrarily. Fig. 9b shows the currents at the next quarter period $\omega t = \Omega_0 + \pi/2$. Assuming that the reference phase Ω_0 was chosen properly, a good CP patch antenna would have vertical fields at $\omega t = \Omega_0$, while the fields for $\omega t = \Omega_0 + \pi/2$ would be horizontally directed. The rotation (RH or LH) can be determined by following the rotation of the fields and noting that the fields radiate out of the page. We see these electric current features exhibited by the distributions plotted in Fig. 9. At $\omega t = \Omega_0$, most of the currents are $\hat{x}$ directed, while at $\omega t = \Omega_0 + \pi/2$ the currents are primarily $-\hat{y}$ directed. The rotation of the currents indicates that this E-shaped patch design radiates LHCP waves. It should also be acknowledged that the currents in Fig. 9a ($\omega t = \Omega_0$) do exhibit other components in the bottom half of the CP E-shaped patch. At this bottom half, the currents appear directed towards the $-\hat{y}$ direction, but the magnitude and the area of these currents is small enough such that the radiation from this current distribution would be dominantly $\hat{x}$ directed. It is important to note that the typical electric surface currents for the LP E-shaped patch are $\hat{y}$ directed, while the strong J_x currents are newly introduced in the asymmetric design, as indicated in Fig. 9a. A last interesting observation is that the CP action happens primarily within the area denoted with the dashed box. A closer look reveals that the dimensions of the patch within this geometry (illustrated by the lengths ℓ_x and ℓ_y) are near resonant. These dimensions are typically close to $\lambda_g/2$ and thus can enable a resonant mode within the patch antenna. The addition of an asymmetry allows a new mode with $\hat{x}$ directed currents to be excited, and the resonant length ℓ_x is adjusted to control the mode's phase. If 90° is achieved, then good CP performance can be achieved.

An important question arises from these observations: how does this patch enable wideband CP patch operation? Just as was demonstrated with LP patch antennas, using thick substrates is the primary tool that can offer wider bandwidths. This was first discussed in seminal works such as [18], [19] and revisited theoretically in [3], [20]. There are, however, some important distinctions for CP patch antennas in contrast with LP patch antennas. First, the bandwidth for CP patch

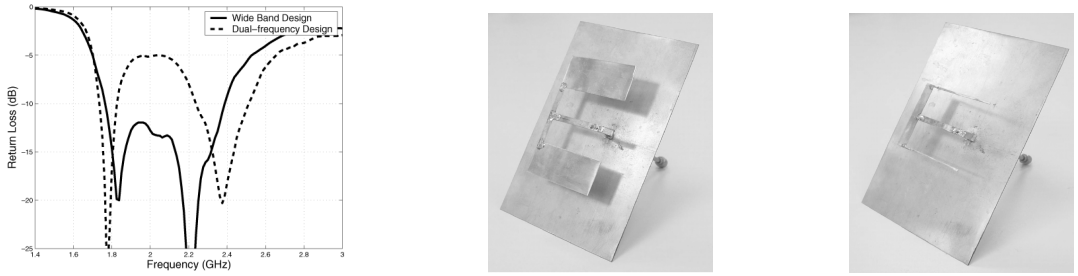

FIGURE 6. (a) Impedance matching performance of dual-band and wideband examples of the E-shaped patch antenna. Geometry is specified in Table 1. (b) Prototype of the wideband design. (c) Prototype of the dual-band design. The air substrate thickness is $t = 15$mm. Adapted from [13].

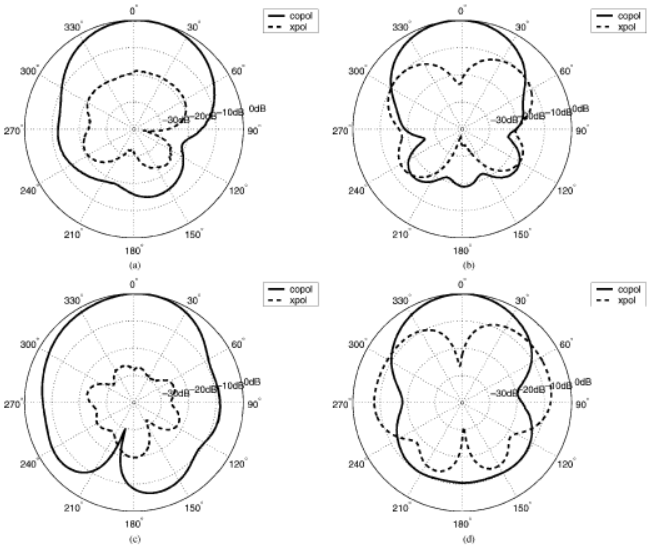

FIGURE 7. Radiation patterns of the wideband E-shaped patch design in Fig. 6b. (a) E-plane, 1.85 GHz. (b) H-plane, 1.85 GHz. (c) E-plane, 2.2 GHz. (d) H-plane, 2.2 GHz. Adapted from [13].

antennas must include both $S_{11} \leq -10$dB and $AR \leq 3$dB, where AR is the axial ratio describing the circularity of the radiated fields. Second, typical single-feed, single-layer CP patch antennas—such as the truncated corner patch design—create CP radiation using two degenerate modes. Each of these degenerate modes radiate a certain orthogonal linear polarization, and a proper feed placement excites both modes with equal amplitude and quadrature phase for CP operation. Given these considerations, it has been proven that the maximum AR-S_{11} bandwidth for a single-feed, single-layer can be predicted by

$$BW_{CP} \approx \frac{\sqrt{2}-1}{Q\sqrt[4]{2}} \approx \frac{0.35}{Q} \tag{4}$$

where Q is the quality factor of each degenerate mode being excited within the patch antenna [3], [20]. Similarly with LP patch antennas, increasing the substrate thickness will directly decrease the quality factor Q of the two orthogonal modes. Equation 4 indicates that the decrease in Q ultimately leads to an increase in bandwidth.

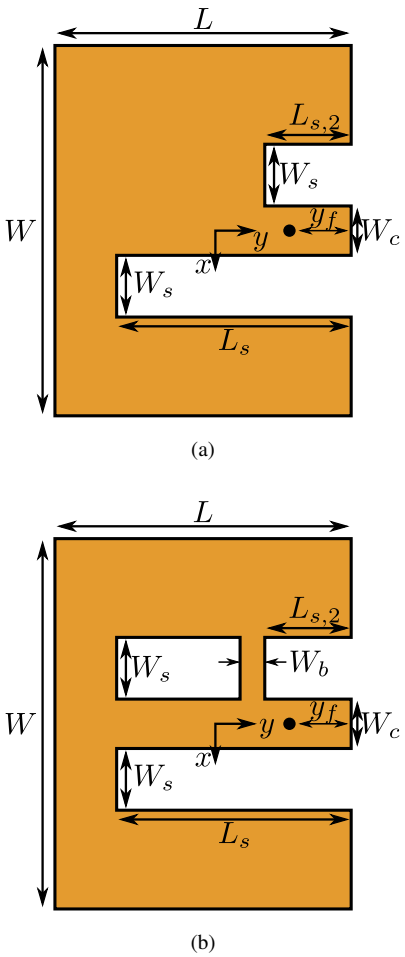

FIGURE 8. (a) A modified E-shaped patch that produces circular polarization (CP) through asymmetric slots [16]. (b) Obtaining CP using a shorting bar across one of the slots [12], [17]. Both versions radiate LHCP.

As we saw with the original LP E-shaped patch antenna, enabling thick substrates allows designers to increase bandwidth. Many of the first CP E-shaped patch antennas discussed in literature demonstrated wideband CP operation, where AR-S_{11} bandwidths on the order of 8-9% were observed for a thickness near $0.09\lambda_0$ [12], [16]. We repeat the results from [12] to demonstrate the performance of

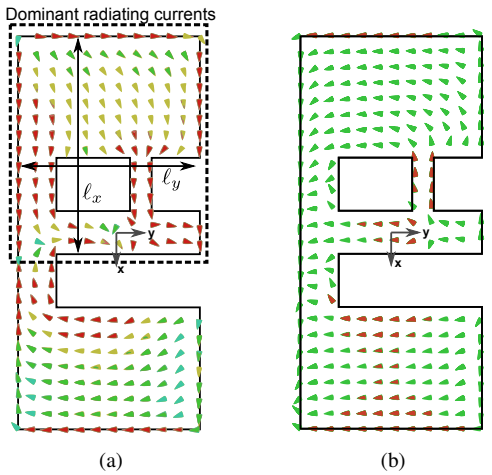

FIGURE 9. Vector plots of the electric surface currents $\mathbf{J}_s$ for a typical CP E-shaped patch using the shorted bar approach. (a) $\omega t = \Omega_0$, showing a mode that primarily radiates an x-directed electric field. (b) $\omega t = \Omega_0 + \pi/2$, showing a mode radiating y-directed electric fields.

such a design. The simulated and measured performance for the previously designed CP E-shaped patch is shown in Fig. 10. In this case, the design was RHCP, and both impedance matching and AR were optimized using PSO. Simulations indicate good CP performance for the band 2.4–2.65 GHz (9.9%), while the AR performance was shifted for the measurement. This decreased the operational band to 2.45–2.6 GHz (8%), the primary reason being the AR contamination from the antenna positioner. The design shown in [16] was able to squeeze out slightly more CP bandwidth, providing roughly 9.3%. The CP E-shaped patch also appeared to achieve slightly higher bandwidths compared with other thick-substrate CP patch antennas. A nice comparison table can be found in [21], where AR-S_{11} bandwidths ranged from 4%–7.6%.

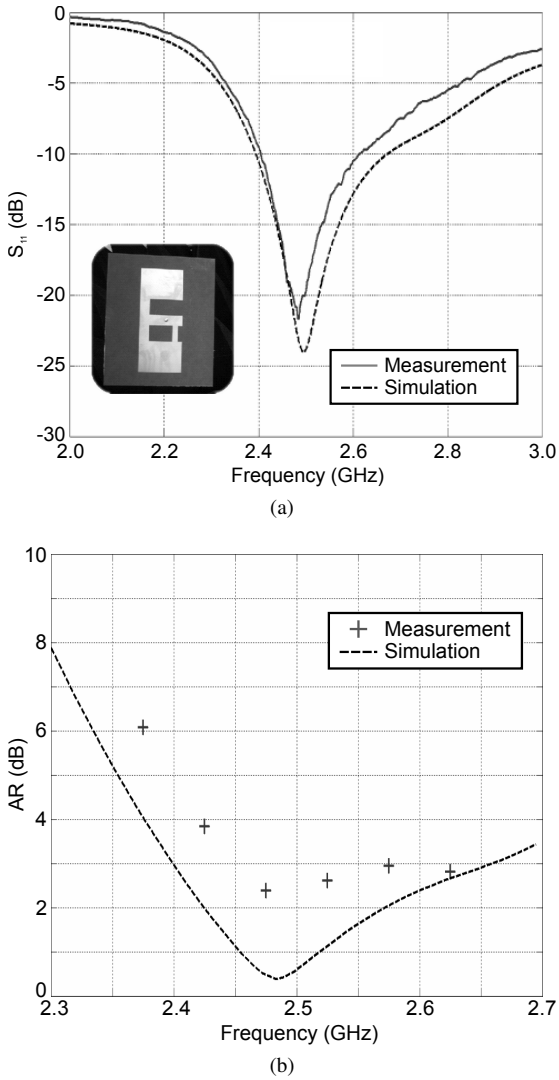

FIGURE 10. Simulated and measured performance of the optimized, RHCP CP E-shaped patch antenna using a shorting bar approach. (a) Impedance matching. (b) Broadside axial ratio (AR). Adapted from [12].

IV. MINIATURIZATION

The previous E-shaped patch antennas have demonstrated wide bandwidths that are useful in many applications. A major caveat of the E-shaped patch antennas is the large width W that comes after careful tuning of the geometry. A large W occurs for both linearly-polarized and circularly-polarized versions of the E-shaped patch. This size limits the practical use of the E-shaped patch, especially for space-constrained applications. A popular example would be an antenna array, where a center-to-center element spacing on the order of $0.5\lambda_0 - 0.8\lambda_0$ is required. With a larger spacing, there is a risk that undesirable grating lobes appear in the radiation pattern.

This limitation encouraged researchers to seek out ways to miniaturize the E-shaped patch concept. In this section, miniaturized versions of both the linearly-polarized and circularly-polarized E-shaped patch antennas are presented. In each case, the size is reduced to nearly half of the original size. There is, of course, a tradeoff with other performance metrics such as cross-polarization. These are discussed in detail in the following subsections.

A. LINEARLY POLARIZED HALF E-SHAPED PATCH

The E-shaped patch antenna has a distinct symmetry about the y-axis as seen in the previous sections. Since the electric surface currents are parallel to this line of symmetry, this means that the currents will be mirrored about the y-axis. The same is also true for the electric fields. These observations lead to an interesting question: can we miniaturize the E-shaped patch by inserting some form of symmetry boundary condition? Theoretically, if we placed a symmetric boundary condition at the y-z plane, then we could remove one half of the E-shaped patch (top or bottom). Even though we only operate with one half of the E-shape, the symmetric boundary condition forces the fields to behave as if the rest of the half-space was mirrored about the y-z plane. Of course, this becomes a problem to implement practically, so

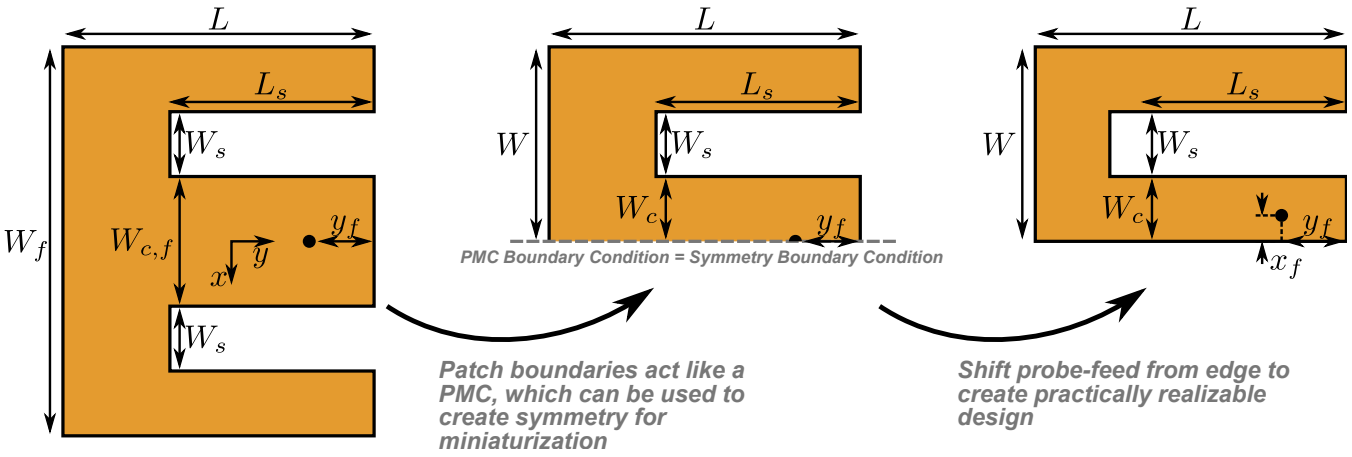

FIGURE 11. Illustration on how to achieve miniaturization in the linearly-polarized E-shaped patch antenna. The Half E-shaped patch gains roughly 50% size reduction compared to the original linearly-polarized E-shaped patch.

naturally the next question for ourselves is how to practically implement the symmetric boundary condition to miniaturize the E-shaped patch.

To answer this question, we will first review the basic operation of patch antennas. Patch antennas operate as a cavity resonator, where fields strongly oscillate underneath the patch shape. During the oscillations, the fields lose energy to intentional radiation in addition to heat. The cavity model for patch antennas fundamentally asserts that any given patch antenna shape behaves as a cavity with perfect electric conducting (PEC) top/bottom walls and perfect magnetic conducting (PMC) boundaries along the periphery of the patch antenna. It is also known that a PMC boundary condition forces a mirrored symmetry, where the total magnetic field must be normal to the surface (zero tangential magnetic field).

A practical realization of the symmetric boundary condition that we seek is to literally cut the patch shape in half along the y axis and discard one of the halves. This places a PMC boundary condition along the line of symmetry for the area defined by $-L/2 \leq y \leq L/2, 0 \leq z \leq h$. If we had perfect PMC boundary conditions for this along the patch antennas, then the half E-shaped resonator would have an identical current distribution as the full E-shaped resonator. While this cavity resonator model is only approximate in the case of a patch antenna, it serves as a nice illustration to understand this miniaturization technique. The PMC concept is illustrated in Fig. 11, where the PMC boundary allows us to cut the E-shape in half. It should be noted that another step must be taken after cutting the patch in half: the probe must be readjusted to accomodate a complete probe (not a probe that is cut in half!). This can be accomplished by positioning the probe in the vicinity of the original probe location.

Not all of the Half E-shaped patch antenna's characteristics are identical to that of the original E-shaped patch antenna. The impedance matching between the two is similar because the PMC boundary condition applies to the inside of the patch antenna. Outside the patch antenna, there is no PMC boundary condition, which means that identical field radiation is not obtained. In essence, the radiation patterns between the Half E-shaped patch and the full E-shaped patch have differences. The primary difference in the radiated field is a slightly higher level of cross-polarization and a wider beamwidth in the H-plane. The patterns can also become asymmetric in the H-plane. The smaller size also leads to a lower broadside directivity for the Half E-shaped patch, which is on the order of roughly 1 dB based on previous results [22]. Previous comparisons have observed 10 dB beamwidths $\approx 100^\circ$ for the full E-shaped patch and $\approx 130^\circ$ for the Half E-shaped patch [22]. For most applications, these changes are not dramatic enough to preclude their use, and we provide an example to demonstrate their performance. In array applications, for example, many of these changes become overshadowed by the array factor.

TABLE 3. Design parameters for a linearly-polarized Half E-shaped patch design (units in mm) [22]

L	W	L_s	W_s	W_c	y_f	x_f
45.0	35.0	32.0	6.0	5.0	14.0	N/A

We highlight an example design using a similar height and size as our previous E-shaped patch antenna designs. The height of the patch antenna is 10mm using a foam (air) substrate, which is roughly $0.087\lambda_0$ at 2.6 GHz. Table 3 provides the dimensions of the Half E-shaped patch antenna that was developed in [22]. The resulting measured performance of the half E-shaped patch is highlighted in Figs. 12-13. The impedance matching (VSWR) performance indicates good performance for the frequency band 2.25-2.9 GHz, providing an impedance matching bandwidth of 25.2%.

The radiation patterns also meet expectations, which can be seen in Fig. 13 for 2.5 GHz. The cross-polarization levels

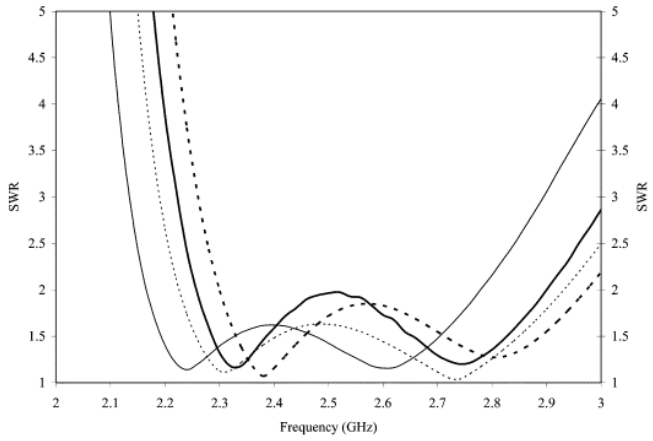

FIGURE 12. VSWR performance of a linearly-polarized half E-shaped patch antenna and its corresponding E-shaped patch where $W_f = 2W$. — half E-patch (measured), - - - half E-patch (simulated), — full E-patch (measured), - - - full E-patch (simulated). Adapted from [22].

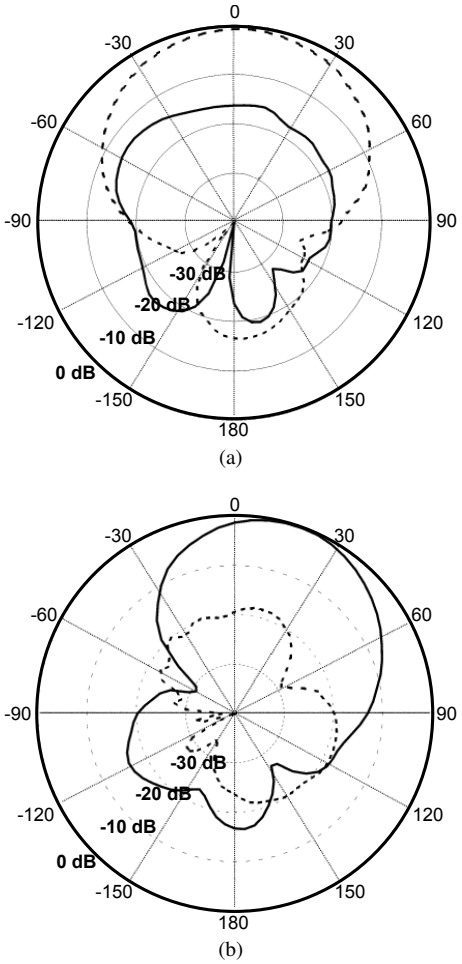

FIGURE 13. Measured radiation patterns of the half E-shaped patch at 2.5 GHz. — E_θ, - - - E_ϕ. (a) x-z plane. (b) y-z plane. Adapted from [22], where we have flipped the patterns according to the coordinate system in Fig. 11.

are less than -18 dB for both x-z and y-z planes. The E-plane (y-z plane) has a larger cross-polarization than the typical E-shaped patch antenna. This occurs because the patch no longer has symmetry about the y-axis, and the cross-polarized currents no longer cancel at $\theta = 0$. Despite this, the cross-polarization remains at reasonable values that are not alarming for a patch in its class. As we mentioned previously, the beamwidth in the H-plane (x-z plane) is a bit larger than the typical E-shaped patch, where the 10 dB beamwidth of the co-polarized fields (E_ϕ) have a 10 dB beamwidth of $\sim 130°$.

B. CIRCULARLY POLARIZED HALF E-SHAPED PATCH

A compact version of the linearly-polarized E-shaped patch was shown in previous section, where the E-shape was cut in half. This design was called the Half E-shaped patch antenna and was able to produce a similar impedance matching bandwidth with a smaller size. Both the original E-shaped patch and the Half E-shaped patch are linearly-polarized. Since we were able to achieve circular-polarization for the CP E-shaped patch antenna, it is only natural to investigate techniques that employ similar ideas to achieve miniaturization for the CP version of the E-shaped patch antenna. The CP E-shaped patch was also among the widest of the E-shaped patch antennas, which posed problems for integration into arrays. This motivated significant interest to apply the miniaturization techniques to the CP version as well. It was observed, however, that obtaining circular polarization in these designs is another problem altogether.

The design shown in Fig. 14 shows the circularly polarized version of the Half E-shaped patch. By adding a new shorting bar of width W_b into the Half E-shaped patch, a mode with currents in the x direction can be excited. Without this shorting bar, the dominant electric-field radiation is in the y direction. To obtain good AR, a proper adjustment of the bar width and position within the slot is required to ensure that both modes are being excited equally. The current distribution shown in Fig. 15 highlights these points. The currents are shown for two points in time $\omega t = \Omega_0$ and $\omega t = \Omega_0 + \pi/2$, where Ω_0 is the reference phase which can be chosen arbitrarily. The y-directed mode dominates for the first time instance, and the x-directed mode dominates the currents in the second time instance. Equal magnitudes between the x and y components is an important feature for CP radiation, and Fig. 15 indicates that both x and y directed current modes have similar magnitudes. We also tested the effect of removing this shorting bar, which effectively create a linearly polarized Half E-shaped patch antenna. In short, our results demonstrate poor AR performance without this shorting bar.

There are many important advantages to this CP Half E-shaped patch design. Much like the CP E-shaped patch design, we are enabling thicker substrates to be utilized. The thicker substrates enable a broad bandwidth to be obtained than typical bandwidths obtained by single-layer, single-feed designs. The CP Half E-shaped patch design in Fig. 14 also

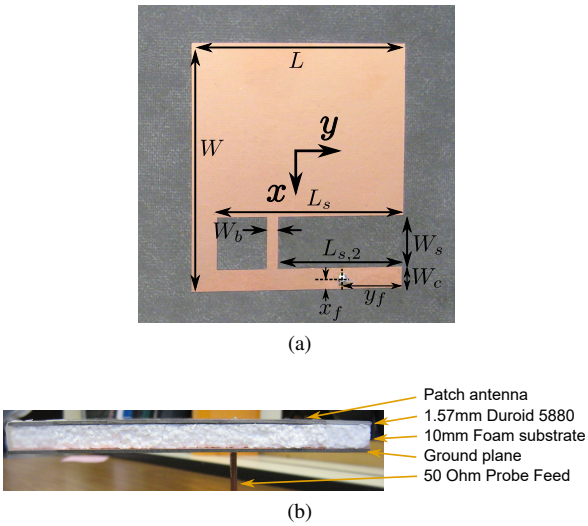

FIGURE 14. Geometry of the CP Half E-shaped patch. (a) Top view of the prototype. (b) Side view showing the layer stackup. Adapted from [21].

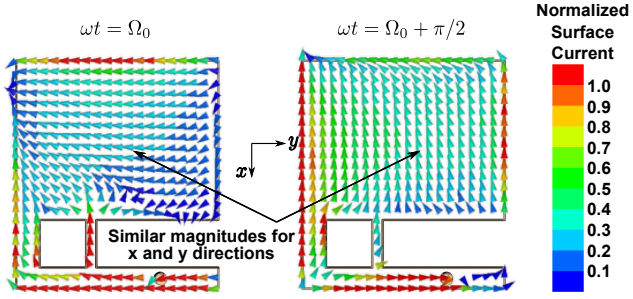

FIGURE 15. Simulated electric surface current vectors on CP Half E-shaped patch for two time instances to demonstrate circular polarization at 2.45 GHz. Adapted from [21].

does not require multilayer fabrication processing and the gap sizes are reasonable with respect to the wavelength ($\sim 0.1\lambda_0$-$0.2\lambda_0$). This potentially provides an advantage over designs such as the CP L-shaped probe [23] and modified truncated-corner CP patch antennas [20]. The CP Half E-shaped patch antenna can be fabricated using low-cost PCB processes alone. When this design was fully reported in [21], a major interest was to scale the design to X-band or higher since small gaps are avoided. This has many advantages, and an X-band prototype was actually demonstrated in a recent array application [24].

To demonstrate the broadband and miniature capabilities of this antenna, an example prototype is provided in Fig. 14. The prototype's top metallic layer and layer stackup are shown in Fig. 14. This design employed a 1.57mm Rogers Duroid 5880 substrate mounted atop a 10mm foam substrate, as seen in Fig. 14b. At a design frequency of 2.45 GHz, the electrical thickness of the stackup is $0.09\lambda_0$.

Nine geometrical parameters must be tuned for proper CP patch antenna operation, making this an intensive design optimization. A proper design flow for this CP patch has

TABLE 4. Design parameters for a CP Half E-shaped patch design (units in mm) [21]

L	W	L_s	$L_{s,2}$	W_s	W_c	x_f	y_f	W_b
49.0	55.1	43.3	29.3	11.8	4.76	2.17	13.8	2.5

yet to be fully investigated for the CP Half E-shaped patch, but a good starting point using an equivalent diagonally-fed nearly-square patch has been discussed in [25]. When first investigating this design, PSO was employed to explore the capabilities of the CP Half E-shaped patch. We optimized the parameters to provide the good broadside AR, S_{11}, and AR-S_{11} bandwidth, similarly to the procedure applied in [17]. The final, optimized geometrical values are given in the caption of Table 4.

Our following performance measurements found that the CP Half E-shaped patch can achieve a broad AR-S_{11} bandwidth. The measurements of the S_{11} and the broadside AR are shown in Fig. 16, where an AR-S_{11} bandwidth of 5.3% resulted. Very good impedance matching performance was also obtained, where the measured S_{11} remains ≤ -20 dB over the band of interest. In fact, the measured $S_{11} \leq -10$ dB bandwidth extends from 1.89–2.7 GHz, roughly 35% bandwidth. This could be also be useful for applications which do not have a preference on polarization.

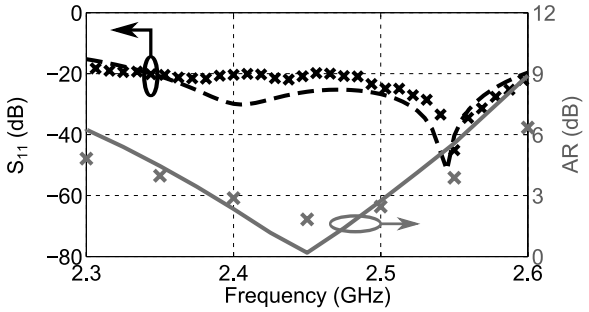

FIGURE 16. Measured impedance matching and broadside AR performance of the CP Half E-shaped patch antenna prototype shown in Fig. 14. Measurements and simulations shown with × markers and solid lines, respectively. Adapted from [21].

There were also no surprises in the measured radiation pattern performance, which appeared fairly similar to other CP patch antennas with thick substrates. The pattern performance for 2.45 GHz can be found in Fig. 17. The directivity for 2.45 GHz was roughly 9.67 dB with an AR of 1.95 dB. Note that a ground plane size of 15×15cm was used in order to shield the interactions with the AUT positioner in the spherical near-field measurement chamber. As with all thick substrate patch antennas, the cross-polarization levels increase fairly quickly for non-broadside angles. Beam squints can also be observed in the radiation patterns, but these are fairly common when using thick substrates. The cross-polarization for this particular radiation pattern measurement was -12 dB below broadside. Similar radiation

pattern performance was also observed at the upper and lower frequencies within the 5.3% bandwidth.

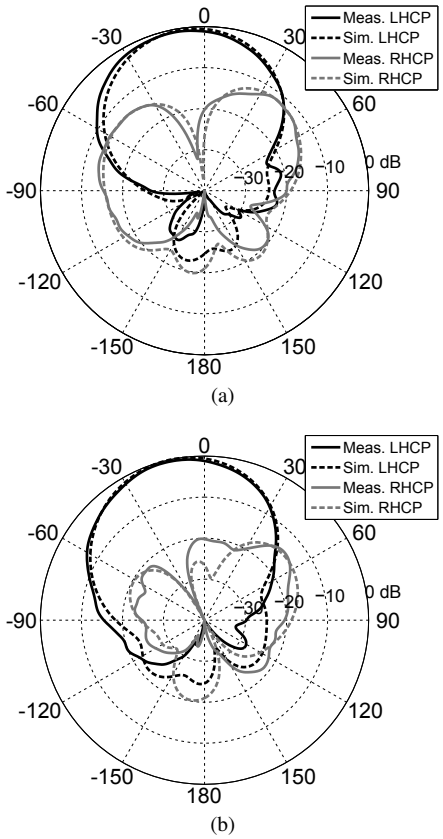

FIGURE 17. Radiation patterns for the CP Half E-shaped patch antenna prototype at 2.45 GHz. (a) $\phi = 0^\circ$ (XZ plane) (b) $\phi = 90^\circ$ (YZ plane). Adapted from [21].

V. RECONFIGURABILITY

Another exciting development for E-shaped patch antennas is the possibility to be made reconfigurable. In general, a reconfigurable antenna is an antenna that can rearrange its internal currents to adjust its frequency characteristics, radiation pattern, or its polarization. In this section, two classes of reconfiguration will be discussed: frequency reconfiguration and polarization reconfiguration. The first class, frequency reconfiguration, is manifested as the ability to switch between two frequency bands of operation. The polarization reconfigurable E-shaped patch that is discussed can switch between two CP modes of operation: RHCP and LHCP. Both exhibited wide bandwidths, which improved the current state-of-the-art for reconfigurable patch antenna technology.

Reconfigurability is achieved by altering the physical path for electric currents to travel. This can be accomplished by alter the antenna's structure through electronic, mechanical, or material means. Electronic changes are by far one of the most popular strategies for reconfigurability, with a big motivation being the short switching time between multiple states. Within the category of electronic switches, varactors, PIN diodes, and FETs are often the most popular for reconfiguring an antenna. Microelectromechanical system (MEMS) switches are another interesting technology that has gained attention over the past two decades. The excitement primarily drew from the low insertion loss and the high power handling capabilities of MEMS switches. The next sections discuss how frequency and polarization reconfigurability can be implemented using MEMS switches. These designs are not necessarily limited to this technology; they could easily be extended using a number of other electronic switches.

A. FREQUENCY RECONFIGURABILITY

The sensitivity of the E-shaped patch antenna to its slot geometry offers straightforward path for adding reconfigurability. The primary advantages include easy accessibility of the slots for bias lines to control the active switches and a low number of switches (only two are used). A low number of RF switches leads to a lower level of complexity

As mentioned in the previous sections, the E-shaped patch antenna has two modes of operation the slots introduced into the rectangular patch topology. These slots which create the E-shape allow another mode to resonate at a lower frequency relative to the typical patch mode. This is due to the currents resonating over a longer geometrical path as shown in Fig. 18b. This mode has strong dependence on the slot geometry (Fig. 18b), while the normal patch mode depends primarily on the patch resonant length (Fig. 18a). This patch resonant length is often given by $\lambda_g/2$, as shown in Fig. 18a. Changing the slot dimensions strongly controls the resonant modes of the E-shaped patch, and therefore they can be altered to provide a desired impedance matching performance. The slot length in Fig. 18c is shortened in comparison to Fig. 18b, and consequently the current has a smaller distance to travel around the slots, giving rise to a higher resonant frequency. If somehow these slot lengths could be changed dynamically, the E-shaped patch antenna could achieve frequency reconfigurability. The burning question then is how to use RF switches to dynamically change the slot length.

It would be very difficult to continuously change the slot length L_s with ON/OFF RF switches. With a discrete number of switches, we can change the slot length in discrete steps. Since a major emphasis of this work was design simplicity, only one switch was implemented in each slot, as shown in Fig. 18d. These two MEMS switches implemented a binary change in the slot length, where the hope was that the binary change would lead to two states providing a wide bandwidth functionality. If wideband performance (roughly 25% bandwidth) could be maintained in each state, then a very wideband frequency support could be obtained with this patch antenna.

Designing such a structure involves tuning for two operational states, representing a multiobjective optimization problem. This makes it more difficult to tune manually, and thus PSO was applied to this frequency reconfigurable E-shaped patch design. A major challenge embedded in this optimization was that the two different switch states cannot

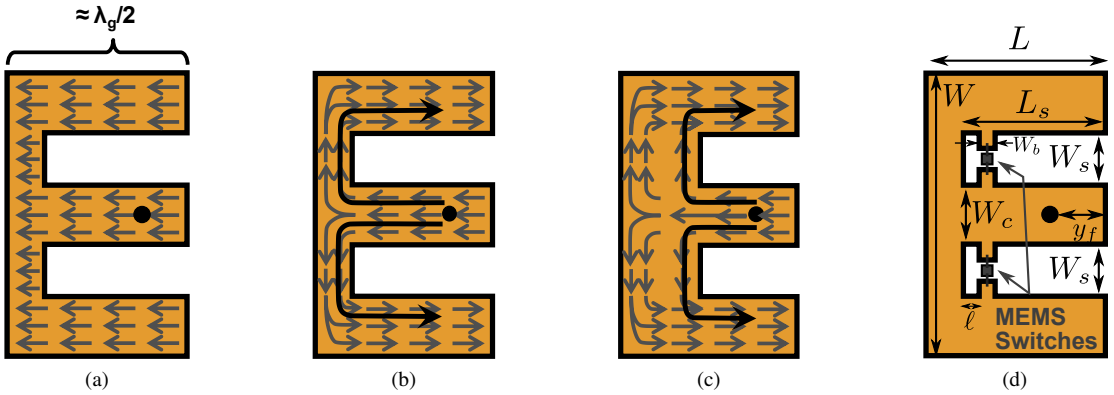

FIGURE 18. (a) Radiating patch mode currents. (b) Non-radiating slot mode currents. (c) Changing the slot dimensions to change the resonant length of the E-shaped patch antenna. (d) Frequency reconfigurable E-shaped design with MEMS switches. Adapted from [26].

TABLE 5. Optimized Geometry (in mm) for the Frequency Reconfigurable E-shaped Patch [26]

W	L	L_s	W_s	W_c	W_b	y_f	ℓ
95.9	44.3	28.6	11.4	14.8	2.5	3.55	4.88

be independently tuned. Changes that enhance one operational state might degrade performance in the other mode of operation. With that observation, it was very important to ensure that both states received equal attention by the optimizer in order to ensure good operation in both states. The goal of the optimization was to optimize the impedance matching for the bands 2-2.6 GHz for the OFF state and 2.6-3.25 GHz for the ON state. PSO was linked with Ansys High Frequency Structure Simulator (HFSS) in order to simulate the S_{11} performance, and the port data from HFSS was extracted and processed by PSO. The MEMS switches were modeled in the OFF and ON states as a lumped element capacitor and resistor, respectively. This simplified model provided decent agreement with measurements while, more importantly, keeping simulation time low. Interested readers can find further details of the optimization given in [26]. The final design parameters given by PSO is given in Table 5.

The final optimized design was fabricated on a thin 0.787mm Rogers Duroid 5880 board placed above a 10mm foam substrate. The ground plane was removed on the bottom of the Rogers substrate and another ground plane was placed on the foam. The layer stackup is identical to that shown in Fig. 14b for the CP Half E-shaped patch antenna. This layer stackup gave us the detailed accuracy of a chemical etching process while allowing thick quasi-foam substrates. It also allowed a solid substrate amenable to mounting the MEMS switches. The Radant MEMS RMSW100HP switches were used to implement the RF switch functionality, where their availability and good switch performance played a major factor in the decision to use them. These RF-MEMS switches were placed and wirebonded to the prototype shown in Fig. 19 in order to test the performance with active switches. Bias lines were implemented using a resistive ink (Ted Pella Isopropanol Graphite Paint) to provide the actuation voltage to the MEMS. This resistive ink had a high sheet resistance of 2400 Ω/sq, which enabled good isolation between the RF and DC actuation circuits. It also removed the high coupling that occurred between the lines and the patch if metal wires were used, which is discussed in detail in [27].

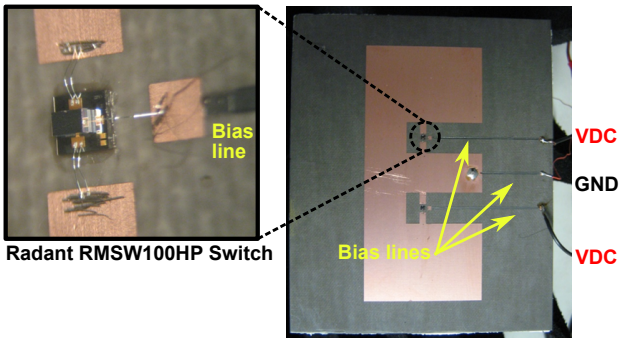

FIGURE 19. Fabricated final optimized frequency reconfigurable E-shaped patch antenna with MEMS switches and a resistive bias line network to minimize interference between the bias lines and the antenna. Adapted from [26].

The fabricated antenna demonstrated wideband features in both its impedance matching and radiation patterns. Fig. 20 provides a comparison of the measured S_{11} results between the wirebonded MEMS measurement and the circuit model for both states. In the OFF state, where both MEMS switches are OFF, we see good impedance matching ($S_{11} \leq -10$dB) over a 2-2.6 GHz bandwidth, which was the intention when the design was optimized. This leads to roughly 26% bandwidth (centered at 2.3 GHz) for this particular state, which is a nicely wideband performance. In the ON state, where both MEMS switches are ON, good impedance matching is obtained over 2.6-3.25 GHz bandwidth This gives roughly 22.3% bandwidth centered at 2.92 GHz. Based on these results, this antenna can support frequencies over the entire range of 2-3.25 GHz, assuming the appropriate mode is

chosen for the operational frequency. Such a wide bandwidth gives roughly 50% bandwidth, which is an incredibly wide supportable bandwidth for a patch antenna.

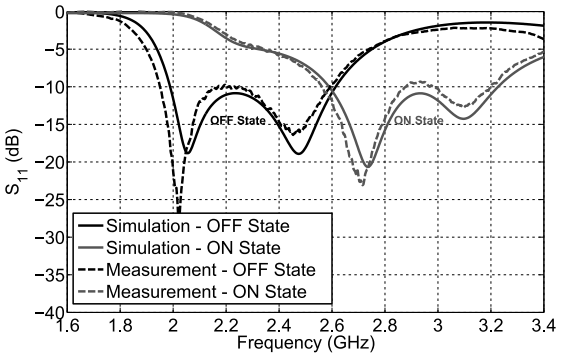

FIGURE 20. Simulated and measured impedance matching performance for the final optimized frequency reconfigurable E-shaped patch antenna including the bias lines. Adapted from [26].

The radiation patterns also were typical of patch antennas, where most of the radiation was directed towards broadside ($\theta = 0$). In Fig. 21, we show several representative patterns for the antenna in both modes of operation at different frequencies. The first patterns in Figs. 21a-b show the patterns for the OFF state at the lower end of the operating band: 2.05 GHz. The second pair of patterns in Figs 21c-d illustrate the patterns for the ON state at 2.8 GHz. While both sets of patterns exhibit features fairly common for patch antennas, a quick comparison between the pairs of patterns reveals a slightly narrower beam for the higher frequency in the ON state. This is to be expected since the antenna grows in electrical size as the frequency increases. One interesting feature is in the H-plane pattern of Fig. 21d, where an increase in cross-polarization is observed. This occurs because the large electrical width of the E-shaped patch leads to higher cross-polarization, where the cross-polarization currents become sufficiently separated in distance so that imperfect cancellation increases the levels.

Regardless, the main feature being sought was the capability to provide wide bandwidth support to access a greater swath of frequencies. This frequency reconfigurable E-shaped patch concept provided a very wide bandwidth with a minimal number of switches. There have been other interesting frequency reconfigurable E-shaped patch antennas proposed in literature. In [28], a frequency reconfigurable dual-band antenna was proposed to provide multiservice functionality. A frequency reconfigurable back-to-back E-shaped patch was theoretically investigated in [29]. Another wideband frequency reconfigurable E-shaped patch antenna was investigated in [30], where 17 switches were used to realize two scaled broadband E-shaped patch antennas. In [31], an interesting frequency reconfigurable half E-shaped patch was investigated for used in multifunctional radio platforms.

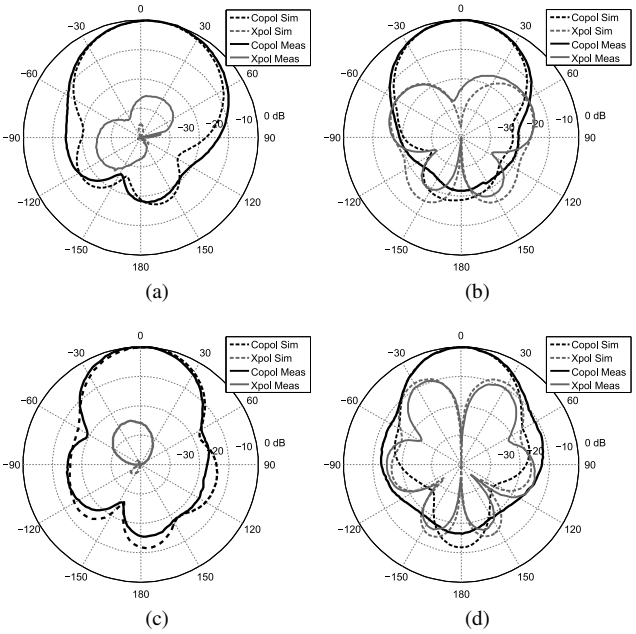

FIGURE 21. Radiation patterns for the final optimized frequency reconfigurable E-shaped patch antenna. (a) OFF state, 2.05 GHz, E-plane. (b) OFF state, 2.05 GHz, H-plane. (c) ON state, 2.8 GHz, E-plane. (d) ON state, 2.8 GHz, H-plane. Adapted from [26].

B. RHCP/LHCP RECONFIGURABILITY

Reflecting on the frequency reconfigurable E-shaped patch antenna discussed in the previous section, a natural follow-up question was how the design performed with only one switch in the ON state. Only turning one switch ON clearly creates an asymmetry in the E-shaped patch structure, bringing the familiar feature that we discussed for CP E-shaped patch antennas without reconfigurability. As illustrated in Fig. 22, turning one switch ON and the other OFF creates an E-shaped patch antenna identical to the CP design presented in Fig. 8b, where asymmetric length slots were created by shorting bars placed across the slot. For the design in Fig. 22, the difference is that there are RF switches (in this case MEMS) that allow the shorting bars to be connected or disconnected dynamically. By dynamically flipping the asymmetry in the slot geometries, the design can operate either as an RHCP radiator or as an LHCP radiator.

There are many similarities between this design and the frequency reconfigurable E-shaped patch design in the previous subsection. Because of these similarities, the previous design approach could also be nicely applied to this design problem as well. The major change to the optimization algorithm was in the fitness characterization, where we changed the goals of the optimizer to focus on getting good S_{11} and AR at 2.4 GHz and then maximizing the bandwidth capabilities of the patch antenna. For this design, bandwidth was specified by simultaneously satisfying $S_{11} \leq -10$dB and $AR \leq 3$dB. The final optimized design produced by PSO is given in Table 6. The RHCP/LHCP reconfigurable E-shaped patch antenna was also fabricated identically to

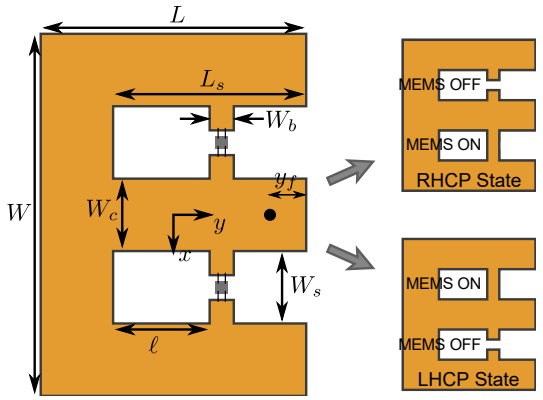

FIGURE 22. Configuration of the MEMS RHCP/LHCP reconfigurable E-shaped patch antenna element to produce either RHCP or LHCP modes. Adapted from [17].

TABLE 6. Optimized Geometry (in mm) for the RHCP/LHCP Reconfigurable E-shaped Patch [17]

W	L	L_s	W_s	W_c	W_b	y_f	ℓ
89.0	45.0	36.0	9.25	5.69	5.0	12.0	15.1

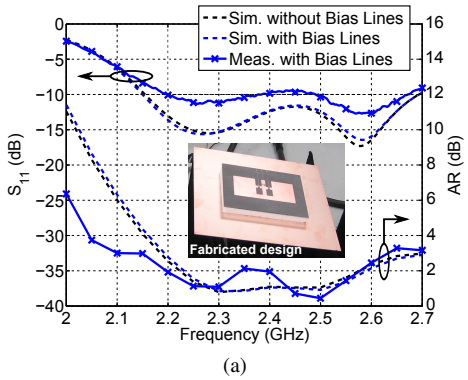

(a)

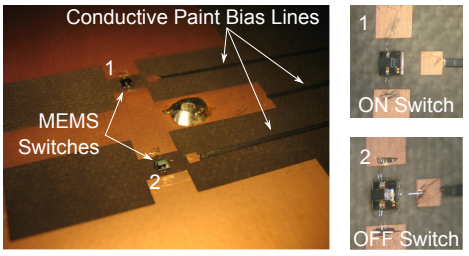

(b)

FIGURE 23. (a) Impedance matching and broadside AR measured performance for the final CP Reconfigurable E-shaped patch. (b) Magnified view of the switch implementation with the conductive paint bias lines. Adapted from [17].

the frequency recofigurable E-shaped patch antenna where the patch shape was etched onto a Rogers Duroid board stacked above a foam substrate. For this design, we used the same MEMS switches, Radant MEMS RMSW100HP, and wirebonded the switches to our antenna. The bias lines also used the same Ted Pella Isopropanol Graphite Paint as a resistive conductor supplying the actuation voltage to the MEMS switches.

The simulated and measured performance for the final reconfigurable CP E-shaped patch design obtained from PSO can be seen in Figs. 23-24. The fabricated design with MEMS switches and bias lines can be seen in Fig. 23. We show the impedance matching performance in Fig. 23, where one can observe the double resonance of the CP E-shaped patch antenna. The errors in fabrication are the primary cause for any discrepancies observed in the measurements, but with a few design iterations to account for these issues, a closer agreement can be obtained. The final design provides roughly 400 MHz AR-S_{11} bandwidth, resulting in a 17% AR-S_{11} bandwidth at 2.4 GHz. Other researchers recently demonstrated a CP reconfigurable E-shaped patch antenna using PIN diodes, but they manually tuned the CP E-shaped patch design resulting in a smaller 7% S_{11}-AR bandwidth [32]. Our design was able to obtain more than double this bandwidth through PSO. Note also that the AR-S_{11} bandwidth is wider than previously observed bandwidths seen in the CP U-slot and the CP L-shaped probe patch antennas. The CP U-slot and L-shaped probe patch antennas seen in [23], [33], [34] typically provide 5-6% AR-S_{11} bandwidth at the same height and similar geometry.

The patterns are shown in Fig. 24 for 2.45 GHz. It should be noted that we used a larger ground plane (200×200mm), as seen in the inset figure of Fig. 23, to remove the impacts of the AUT positioner on the AR, which can be a sensitive measurement. The switch implementation with bias lines is shown in Fig. 23b, where a "thru-line" version was used to test the case with the MEMS ON. Simulations also indicated that this antenna has reasonable efficiencies above 0.95 over the entire operational bandwidth (2.2-2.6 GHz). In these simulations we incorporated the loss tangents and finite conductivity into the HFSS model. For the conductive losses, we utilized the Groisse model with 0.5μm RMS surface roughness and 34μm thickness (corresponding to a 1oz layer of copper). Overall, the characteristics of the patterns are fairly typical of a CP patch antenna. At 2.45 GHz, we obtain roughly 8.35 dBic directivity with an axial ratio of 1.88 dB. The patterns at this frequency show many similarities with those in [32].

VI. APPLICATIONS

Potentially the most rewarding aspect of any research journey is witnessing one's work being applied to real-life systems by others. The E-shaped patch and all of its variations have attracted attention across both research and commercial communities. A number of interesting variations and applications of the E-shaped patch have come to light through publications at various antenna conferences and journals. We have also been notified that E-shaped patch designs have been used extensively in practical applications with no publications reported. We conclude this review article with a reflection on previous, current, and potential future applications of the

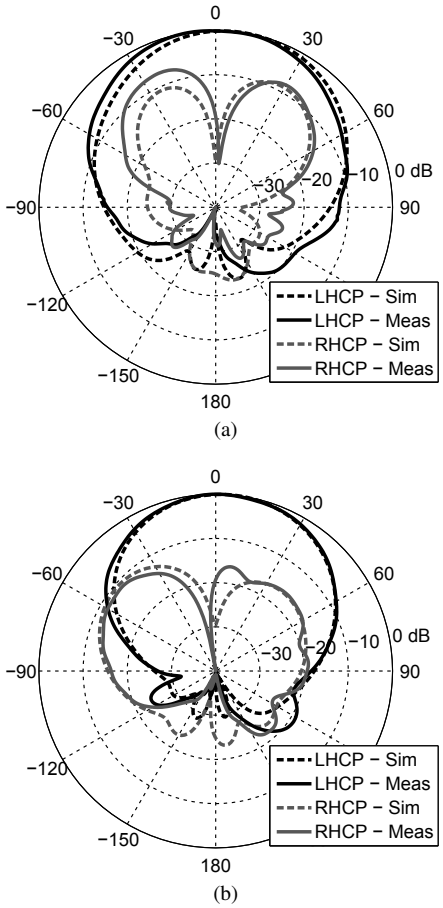

FIGURE 24. Simulated and measured pattern results for the CP Reconfigurable E-shaped patch element. (a) $\phi = 0^\circ$ cut at 2.45 GHz. (b) $\phi = 90^\circ$ cut at 2.45 GHz. Measurements showed a peak directivity of 8.35 dB. Adapted from [17].

E-shaped patch antenna.

The first journal paper that fully studied the E-shaped patch antenna [1] was focused on demonstrating the use of the E-shaped patch for wireless communications. Since that work, many people have investigated the use of E-shaped patch antennas in applications for communications, position-navigation-timing (PNT) systems, and radar. Frequencies of operation focus primarily in the L-band, S-band, and C-bands, although there have been developments that operated in the lower X-band frequencies. Most of the E-shaped patch applications utilized the traditional probe-feeding mechanism, and, as for the substrate materials, most research have either implemented air or foam substrates (although a few have used low dielectric materials like Rogers Duroid 5880LZ).

One of the first follow-up research projects was an investigation to use the E-shaped patch antenna for high-speed wireless networks at the 5-6 GHz frequency range. The idea was to implement a PCMCIA card that could augment current 802.11 WiFi capabilities, which were typically limited to 802.11b operation in the 2.4-2.5 GHz range. New standards were emerging that hoped to employ both 5.15-5.35 GHz and 5.725-5.825 GHz frequency bands, and it is difficult to support both bands with typical patch antennas that fit within the PCMCIA card thickness of 5mm. The researchers developed two arrays for space diversity or decoupled Tx/Rx operation. These arrays are shown in Fig. 25, and further details can be found in [15].

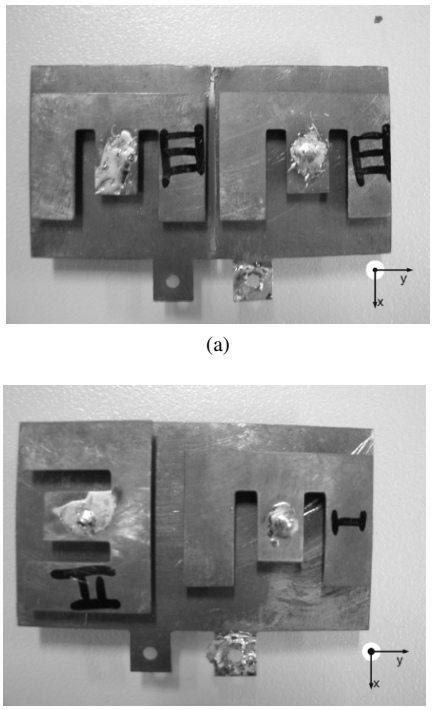

FIGURE 25. E-shaped patch antennas for high speed 5–6 GHz wireless networks. (a) Decoupled antenna array for Tx/Rx duplex. (b) Broadband polarization diversity antenna array. Adapted from [15].

Another interesting usage of the E-shaped patch antenna has been towards realizing wideband arrays. Fig. 26 illustrates a number of different applications where the E-shaped patch was either implemented or studied for use. The first image in Fig. 26a shows highlights an investigation towards their use in through-wall microwave imaging (TWMI), where both wideband RF systems and signal processing could be combined to support rescue missions, behind-the-wall target detection, or even sensing through obscured environments (like smoke or dust). A major challenge in such a system is developing a low-profile array that can support the frequency bandwidth necessary for through-wall detection. The goal was to develop a low-profile array system at 2 GHz with 600 MHz bandwidth. Fig. 26b shows an array of rotated E-shaped patch antenna that provide a wideband CP operation for global positioning systems (GPS). The researchers demonstrated that this combination of E-shaped patches rotated with 90° phase can achieve a wide CP bandwidth, where $S_{11} \leq -10$ dB and $AR \leq 3$ dB was supported for 36% bandwidth centered at 1.68 GHz [36]. More recently, a phase-only null steering array was developed as a low-cost, UHF array that supported a wideband operation [37]. This

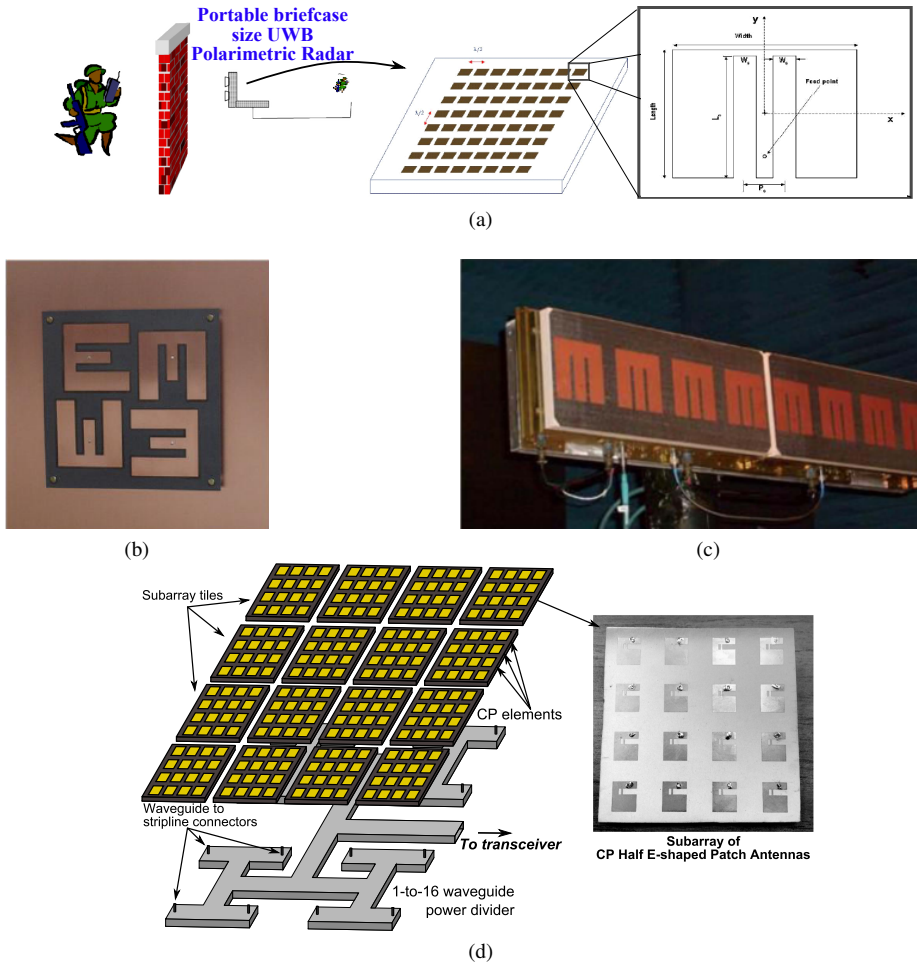

FIGURE 26. E-shaped patch antennas and variations for high performance array applications. (a) E-shaped patch antennas for through-wall microwave imaging (TWMI) at 2 GHz [35]. (b) Sequentially-rotated array for GPS [36]. (c) Wideband null steering array [37]. (d) Array for Direct-to-Earth links for Mars Rovers [24].

null-steering array supported 800-1000 MHz, with a field of view (FOV) of $\pm 60^{\circ}$. The array could steer up to three nulls independently, and the null-steering was accomplished using an analog beamformer. Another recent array development investigated the possibility of implementing a subarray-array of CP Half E-shaped patch antennas for future Mars Rover missions [24]. The hope is to augment current Mars Rover communications by enhancing their Direct-to-Earth (DTE) link, where a new antenna gain of 30 dB represented the next generation of DTE communications. The array of CP Half E-shaped patch antennas aimed to support two narrow frequency bands centered at 7.1675 GHz and 8.425 GHz for Rx and Tx operation, respectively. The authors demonstrated a small 4×4 subarray of CP Half E-shaped patch antennas, which could be integrated into a 16×16 array using a waveguide feed, as seen in Fig. 26d.

Laptops and other portable devices have also presented challenging problems to antenna designers. A major challenge is supporting multiple standards and functionalities (GPS, WiFi, etc.) within a compact package. Furthermore, advanced antenna array capabilities such as MIMO are also a common and important feature that offers notable performance boosts. This was discussed in [38], where a back-to-back E-shaped patch design was proposed to support the WiFi bands for 2.4 GHz and 5.2 GHz. The back-to-back E-shaped patch allows a more omnidirectional radiation pattern to be obtained, which is useful for laptops whose orientation is mostly unknown. This back-to-back E-shaped patch can be seen in Fig. 27, where both antenna evaluation and user interactions were evaluated. For MIMO capabilities, multiple back-to-back E-shaped patch antennas were also evaluated. Interested readers can refer to [38] for further details of the study.

Reconfigurable antennas have been on the cutting edge of antenna technology, and over the past decade there has been a dramatic surge of interest in adaptive and flexible radios. Reconfigurable antennas are naturally suited for these flexible systems, where the hope is to squeeze out as much high-performance functionalities as possible. In [31], reconfigurable antennas were explored for potentially replacing multiband multi-module systems, where reconfigurable antennas would provide some level of out-of-band filtering to

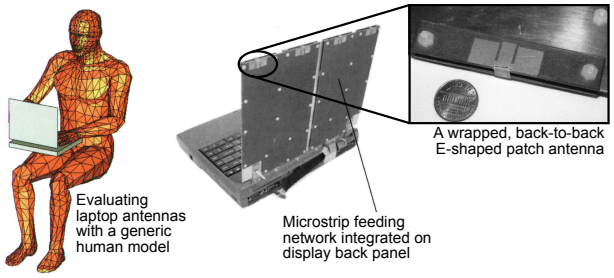

FIGURE 27. Investigations of laptop antennas using a back-to-back E-shaped patch antenna. Both human body interactions and antenna performance evaluation were studied. Adapted from [38].

isolate nearby radios. The use of a Half E-shaped patch antenna was explored to support multiple frequency bands through frequency reconfiguration, where the antenna design is shown in Fig. 28a. Multiradio platforms may not only desire to support multiple frequencies; they may require other electromagnetic modes of operation, namely other polarization features. In [17], [32], wideband polarization reconfigurable E-shaped patch antennas were developed and optimized for wideband performance. Beyond a single element, an array of RHCP/LHCP reconfigurable elements was developed and demonstrated in [17], which is illustrated in Fig. 28b. The element of this array was discussed in the previous section. There has been speculation that one could theoretically achieve a vertical, RHCP, and LHCP in the same antenna element, but so far there has not been any embellishments showing such an operation.

Cognitive radios represent the evolution beyond adaptive radios, where intelligence is added into the radio. The hope is to make the radio aware of its environment, supporting some level of feedback to enable an optimization of system performance. A recent paper on frequency reconfigurable E-shaped patch antennas was discussed in [26], where the aim was to develop a wideband, cognitive radio base station antenna that maintained a low-profile. This was the same frequency reconfigurable design presented in the previous section. As was demonstrated, this antenna maintains a nice wideband performance in every mode of operation, which is potentially useful for spectrum sensing or even communications. A big advantage is that the antenna operational frequencies do not have to be coordinated with the rest of the system.

VII. CONCLUSION

Patch antennas have indeed come a long way since their inception in the late 1950's [39]. It has been very exciting to see an interesting design—the E-shaped patch antenna—attract both scholars and system developers. The excitement has been the wideband (or even dual-band) performance achieved by adding a new mode that cancels the probe reactance. In doing so, many wideband capabilities have been achieved beyond simply wideband linearly-polarized designs. In this review article, we have summarized the developments by many researchers to achieve features like wideband CP performance, miniaturization, and even reconfigurability. We look forward to many more years of progress and applications following the success of the E-shaped patch.

ACKNOWLEDGMENT

The authors would like to thank many of their colleagues who contributed to the development of the E-shaped patch antenna under the supervision of Prof. Rahmat-Samii. Dr. Kovitz's work on the E-shaped patch antennas was done while he was a PhD student at UCLA.

REFERENCES

[1] F. Yang, X. Zhang, X. Ye, and Y. Rahmat-Samii, "Wide-band E-shaped patch antennas for wireless communications," IEEE Transactions on Antennas and Propagation, vol. 49, no. 7, pp. 1094–1100, 2001.
[2] D. R. Jackson, S. A. Long, J. T. Williams, and V. B. Davis, "CAD of rectangular microstrip antennas," in Advances in microstrip and printed antennas, K. F. Lee and W. Chen, Eds. Wiley New York, 1997.
[3] W. L. Langston and D. R. Jackson, "Impedance, axial-ratio, and receive-power bandwidths of microstrip antennas," IEEE Transactions on Antennas and Propagation, vol. 52, no. 10, pp. 2769–2774, 2004.
[4] S. Long and M. Walton, "A dual-frequency stacked circular-disc antenna," IEEE Transactions on Antennas and Propagation, vol. 27, no. 2, pp. 270 – 273, March 1979.
[5] K. Luk, C. Mak, Y. Chow, and K. Lee, "Broadband microstrip patch antenna," Electronics Letters, vol. 34, no. 15, pp. 1442 –1443, July 1998.
[6] T. Huynh and K.-F. Lee, "Single-layer single-patch wideband microstrip antenna," Electronics Letters, vol. 31, no. 16, pp. 1310–1312, August 1995.
[7] S. Weigand, G. Huff, K. Pan, and J. Bernhard, "Analysis and design of broad-band single-layer rectangular U-slot microstrip patch antennas," IEEE Transactions on Antennas and Propagation, vol. 51, no. 3, pp. 457 – 468, March 2003.
[8] S. Bhardwaj and Y. Rahmat-Samii, "A comparative study of C-shaped, E-shaped, and U-slotted patch antennas," Microwave and Optical Technology Letters, vol. 54, no. 7, pp. 1746–1757, 2012.
[9] J. M. Kovitz, "Nature-inspired optimization techniques applied to antennas for wireless communications and radar," Master's thesis, University of California Los Angeles, June 2012.
[10] K. Noguchi, H. Rajagopalan, and Y. Rahmat-Samii, "Design of wideband/dual-band E-shaped patch antennas with the transmission line mode theory," IEEE Transactions on Antennas and Propagation, vol. 64, no. 4, pp. 1183–1192, 2016.
[11] J. Robinson and Y. Rahmat-Samii, "Particle swarm optimization in electromagnetics," IEEE Transactions on Antennas and Propagation, vol. 52, no. 2, pp. 397–407, 2004.
[12] Y. Rahmat-Samii, J. M. Kovitz, and H. Rajagopalan, "Nature-inspired optimization techniques in communication antenna designs," Proceedings of the IEEE, vol. 100, no. 7, pp. 2132–2144, 2012.
[13] N. Jin and Y. Rahmat-Samii, "Parallel particle swarm optimization and finite-difference time-domain (PSO/FDTD) algorithm for multiband and wide-band patch antenna designs," IEEE Transactions on Antennas and Propagation, vol. 53, no. 11, pp. 3459–3468, 2005.
[14] A. Deshmukh and G. Kumar, "Compact broadband E-shaped microstrip antennas," Electronics Letters, vol. 41, no. 18, pp. 989–990, 2005.
[15] Y. Ge, K. Esselle, and T. Bird, "E-shaped patch antennas for high-speed wireless networks," IEEE Transactions on Antennas and Propagation, vol. 52, no. 12, pp. 3213–3219, 2004.
[16] A. Khidre, K. Lee, F. Yang, and A. Elsherbeni, "Wideband circularly polarized E-shaped patch antenna for wireless applications," IEEE Antennas and Propagation Magazine, vol. 52, no. 5, pp. 219–229, 2010.
[17] J. Kovitz, H. Rajagopalan, and Y. Rahmat-Samii, "Design and implementation of broadband MEMS RHCP/LHCP reconfigurable arrays using rotated E-shaped patch elements," IEEE Transactions on Antennas and Propagation, vol. 63, no. 6, pp. 2497–2507, June 2015.
[18] Y. Lo, B. Engst, and R. Lee, "Simple design formulas for circularly polarised microstrip antennas," in IEE Proceedings H (Microwaves, Antennas and Propagation), vol. 135, no. 3. IET, 1988, pp. 213–215.
[19] W. Richards, Y. Lo, and D. Harrison, "An improved theory for microstrip antennas and applications," IEEE Transactions on Antennas and Propagation, vol. 29, no. 1, pp. 38–46, 1981.

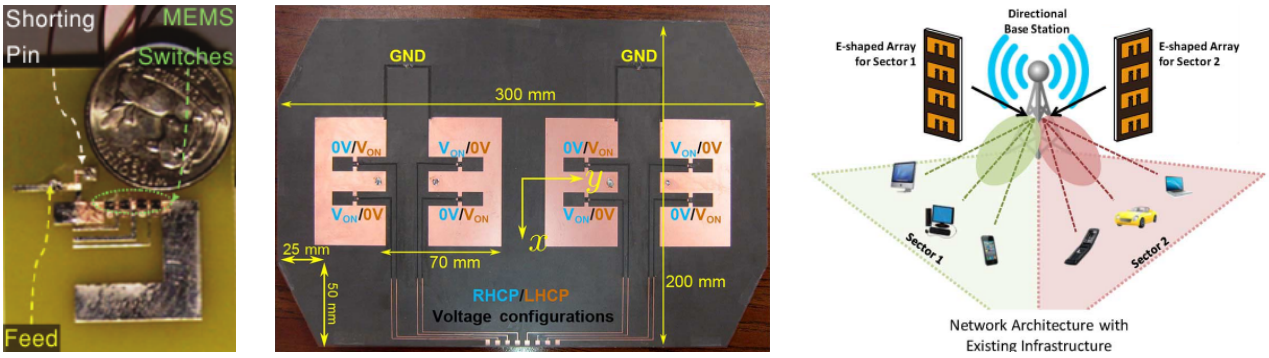

(a) (b) (c)

FIGURE 28. Reconfigurable E-shaped patch antennas and variations. (a) Frequency reconfigurability for multiradio platforms [31]. (b) RHCP/LHCP reconfigurable array for wideband base stations [17]. (c) Frequency reconfigurability for cognitive radio base stations [26].

[20] J. M. Kovitz and Y. Rahmat-Samii, "Using thick substrates and capacitive probe compensation to enhance the bandwidth of traditional CP patch antennas," IEEE Transactions on Antennas and Propagation, vol. 62, no. 10, pp. 4970–4979, Oct 2014.

[21] J. M. Kovitz, H. Rajagopalan, and Y. Rahmat-Samii, "Circularly polarised half E-shaped patch antenna: a compact and fabrication-friendly design," IET Microwaves, Antennas & Propagation, vol. 10, no. 9, pp. 932–938, 2016.

[22] C.-L. Mak, K.-F. Lee, K.-M. Luk, A. Kishk et al., "Miniature wide-band half U-slot and half E-shaped patch antennas," IEEE Transactions on Antennas and Propagation, vol. 53, pp. 2645–2652, 2005.

[23] S. S. Yang, K.-F. Lee, and A. A. Kishk, "Design and study of wideband single feed circularly polarized microstrip antennas," Progress In Electromagnetics Research, vol. 80, pp. 45–61, 2008.

[24] J. M. Kovitz, J. P. Santos, Y. Rahmat-Samii, N. Chamberlain, and R. Hodges, "High-performance circularly-polarized patch subarrays for dual-band direct-to-earth communications in future mars rover missions," IEEE Antennas and Propagation Magazine, vol. 59, no. 3, 2017, to appear.

[25] J. M. Kovitz, "Innovative antenna designs for broadband circularly-polarized wireless systems and software radios," Ph.D. dissertation, University of California Los Angeles, December 2015.

[26] H. Rajagopalan, J. Kovitz, and Y. Rahmat-Samii, "MEMS reconfigurable optimized E-shaped patch antenna design for cognitive radio," IEEE Transactions on Antennas and Propagation, vol. 62, no. 3, pp. 1056–1064, March 2014.

[27] J. M. Kovitz, H. Rajagopalan, and Y. Rahmat-Samii, "Practical and cost-effective bias line implementations for reconfigurable antennas," IEEE Antennas and Wireless Propagation Letters, vol. 11, pp. 1556–1559, 2012.

[28] S. M. Asif, A. Iftikhar, S. M. Khan, M. Usman, and B. D. Braaten, "An E-shaped microstrip patch antenna for reconfigurable dual-band operation," Microwave and Optical Technology Letters, vol. 58, no. 6, pp. 1485–1490, 2016.

[29] J. Guterman, A. Moreira, C. Peixeiro, and Y. Rahmat-Samii, "Reconfigurable E-shaped patch antennas," in IEEE International Workshop on Antenna Technology (iWAT). IEEE, 2009, pp. 1–4.

[30] B. Wang, S. Xiao, and J. Wang, "Reconfigurable patch-antenna design for wideband wireless communication systems," IET Microwaves, Antennas & Propagation, vol. 1, no. 2, pp. 414–419, 2007.

[31] S. Yang, C. Zhang, H. Pan, A. Fathy, and V. Nair, "Frequency-reconfigurable antennas for multiradio wireless platforms," IEEE Microwave Magazine, vol. 10, no. 1, pp. 66–83, 2009.

[32] A. Khidre, K.-F. Lee, F. Yang, and A. Elsherbeni, "Circular polarization reconfigurable wideband E-shaped patch antenna for wireless applications," IEEE Transactions on Antennas and Propagation, vol. 61, no. 2, pp. 960–964, 2013.

[33] K. Tong and T. Wong, "Circularly polarized U-slot antenna," IEEE Transactions on Antennas and Propagation, vol. 55, no. 8, pp. 2382–2385, 2007.

[34] P. Qin, A. Weily, Y. Guo, and C. Liang, "Polarization reconfigurable U-slot patch antenna," IEEE Transactions on Antennas and Propagation, vol. 58, no. 10, pp. 3383–3388, 2010.

[35] V. Komanduri, A. Hoorfar, and N. Engheta, "Wideband printed antenna elements for through-wall microwave imaging applications," in IEEE Sarnoff Symposium, 2004, pp. 61–64.

[36] L. Marzall, D. Lunardi, R. Schildberg, and J. da S Lacava, "Circularly-polarized planar array of sequentially rotated E-shaped elements," in IEEE Antennas and Propagation Society International Symposium. IEEE, 2010, pp. 1–4.

[37] T. Lam, "Null steering antenna array using phase-only weights," in IEEE Antennas and Propagation Society International Symposium. IEEE, 2014, pp. 1660–1661.

[38] J. Guterman, A. Moreira, C. Peixeiro, and Y. Rahmat-Samii, "Wrapped microstrip antennas for laptop computers," IEEE Antennas and Propagation Magazine, vol. 51, no. 4, pp. 12–39, 2009.

[39] G. A. Deschamps and W. Sichak, "Microstrip microwave antennas," in Third USAF Symposium on Antennas, vol. 84, 1953.